Simulation of neutral gas flow in the JET sub-divertor

EUROFUSION WPJET1-PR(16) 16580

S Varoutis et al.

Simulation of neutral gas flow in the JET sub-divertor

Preprint of Paper to be submitted for publication in
Fusion Engineering and Design

This work has been carried out within the framework of the EUROfusion Consortium and has received funding from the Euratom research and training programme 2014-2018 under grant agreement No 633053. The views and opinions expressed herein do not necessarily reflect those of the European Commission.

Simulation of neutral gas flow in the JET sub-divertor

S. Varoutis[1], C. Gleason-González[1], D. Moulton[2], U. Kruezi[3], M. Groth[2], Chr. Day[1], S. Wiesen[4], D. Harting[3] and JET Contributors[*]

EUROfusion Consortium, JET, Culham Science Centre, Abingdon, OX14 3DB, UK

[1]Karlsruhe Institute of Technology, 76344, Karlsruhe, Germany.
[2]Aalto University, Espoo, Finland.
[3]Culham Centre for Fusion Energy, Abingdon, UK.
[4]Forschungszentrum Jülich GmbH, Institut für Energie- und Klimaforschung - Plasmaphysik, 52425 Jülich, Germany.

E-mail: stylianos.varoutis@kit.edu

Abstract. The present work presents a numerical study of the neutral gas dynamics in the JET sub-divertor. A complex model of the sub-divertor geometry is implemented and successful comparisons between corresponding numerical and experimental data have been performed. The experimental data represent the neutral gas pressure obtained by a sub-divertor pressure gauge. The recently developed Divertor Gas Simulator (DIVGAS) which is based on the Direct Simulation Monte Carlo (DSMC) method is applied. DIVGAS is able to predict the behaviour of the flow including macroscopic quantities of practical interest as for instance the pressure, temperature and bulk velocity. For all presented plasma cases, the deduced flow pattern is non-isothermal and covers the free molecular up to the transition flow regime. Furthermore, for low and medium divertor density simulations, recirculation effects occur through gaps between the vertical target tiles, which seem to be two order of magnitude less compared with the recycling ion flux onto the divertor walls.

1. Introduction

Over the last few years much effort has been invested in modeling the neutral gas flow through the complex divertor and sub-divertor region in tokamak fusion reactors [1-4]. The main goal is the investigation of the impact of neutral gas dynamics on the particle removal process and the overall pumping efficiency during plasma operation. Neutral particle dynamics become more important when the plasma behavior is dominated by plasma-wall interactions (i.e. the recycling flux is greater than the deuterium injection by at least one order of magnitude) and/or when the operational regime is strongly dependent on the neutral behavior (e.g. within detached plasma scenarios or due to penetration of neutrals into the core etc.). Depending on the plasma conditions, the ratio of the mean free path to a characteristic length scale of the divertor, the so-called Knudsen number (Kn), may vary over a wide range. This number in a fusion device covers values starting from the continuum ($Kn \to 0$) and slip regimes ($10^{-3} \leq Kn < 0.1$) above the dome and close to the divertor targets, and the

[*] *See the Appendix of F. Romanelli et al., Proceedings of the 25th IAEA Fusion Energy Conference 2014, St. Petersburg, Russia.*

transitional regime ($0.1 \leq Kn < 10$) and even free molecular ($Kn \to \infty$, collisionless) regime in the sub-divertor area and inside the vacuum pumps. Consequently, a reliable estimate of the macroscopic parameters in such a complex system requires a tool to describe the flow in the whole range of gas rarefaction. Currently, to calculate the plasma and neutral conditions in the SOL, the code package which is often used on fluid edge plasma modeling is the EDGE2D-EIRENE code [5], the EDGE2D consists of a 2D plasma fluid code, while the EIRENE algorithm [6] includes a 3D Monte-Carlo solver for neutral-neutral interactions, based on the BGK kinetic model [7,8]. Over the years the EIRENE code has been proven to work sufficiently well in neutral modelling. However, no qualitative and quantitative comparison with a more complete neutral code has yet been performed in the sub-divertor region and under various operational plasma conditions. This statement comprises the motivation of this work. It is noted that the main drawback of the linear BGK approach is the inability to correctly describe simultaneously the transport coefficients of a specific neutral gas i.e. the gas viscosity and the thermal conductivity. It can be deduced that BGK does not provide the right ratio for the transport coefficients, namely the ratio of the thermal conductivity over viscosity. As a result using the BGK model, the obtained Prandtl number for a monoatomic gas is equal to unity instead of 2/3 [8,9]. Therefore, the BGK kinetic model is commonly applied only for pressure driven isothermal flows. To describe more efficiently non-isothermal flows (as expected in the sub-divertor region), the use of the Direct Simulation Monte Carlo method (DSMC) [10] is suggested in the present work.

The DSMC approach is based on a particle method, in which the solution of the Boltzmann kinetic equation is approximated by simulating groups of model particles that statistically mimic the behavior of real molecules. Investigations about neutral gas dynamics in the sub-divertor volume have been performed in the past [11-14], but most of them were focused in low density sub-divertor conditions, where the neutral-neutral collisions do not have a prominent role in the calculation of overall quantities. More recently, a similar investigation on the ITER sub-divertor was performed by successfully implementing the DSMC method coupled with SOLPS input data [15]. It was observed that high recirculation of neutrals behind the divertor targets occur (i.e neutral particles moving backwards to the plasma region). Following this applied workflow, the recently developed Divertor Gas Simulator (DIVGAS), which is a code based on the DSMC algorithm and is capable of modelling neutral gas flows in a tokamak sub-divertor, is applied for all the presented simulations.

The present work mainly focuses on the numerical simulation of the neutral gas flow and the calculation of overall quantities of practical interest i.e. pressure, density, temperature, bulk velocity, recirculation rates etc., inside the complex geometry of the JET sub-divertor by applying the DIVGAS code. For validation purposes, the numerical values are compared with existing JET ITER-Like Wall (ILW) experimental data for the neutral gas pressure distribution in the sub-divertor region presented in [16]. The sub-divertor pressure measurements were obtained with a pressure gauge located at the end of the main vertical lower port of JET Octant 8. The comparison between experiments and numerical data is focused on different L-mode plasma scenarios, which cover a wide range of neutral gas divertor densities. For each case, the corresponding EDGE2D-EIRENE plasma simulations have been performed. Then, the information about the neutral particles on the interfaces along the divertor geometry are extracted and imposed as boundary conditions (BC) for DIVGAS simulations. Following the above steps, the whole range of the Knudsen (Kn) number is being covered and it made possible to quantify the differences between the numerical and experimental results in each regime.

2. Divertor flow configuration

The scope of this work is to examine the 2D behavior of the molecular and atomic deuterium (i.e D_2 and D) binary gas mixture flow inside the JET sub-divertor domain. Fig. 1 illustrates the used 2D-cut of the 3D JET CATIA model of the JET Octant No. 8. The cyan area highlighted in Fig. 1 was chosen as the simulation domain for the DIVGAS calculations. Although the selected geometry is simplified, it still preserves a high degree of complexity of the overall divertor structure, which limits the overall conductance of the system. In addition, the present configuration includes the cryopump and corresponding radiation shielding (louvres), the main lower port duct and the pipes, which connects

the sub-divertor with the pressure gauge position (see Fig. 2a). This is necessary, because, as will be justified further below in this paper, due to the relatively high densities which are expected to appear there, the conductance cannot be easily calculated using available analytical solutions. The water cooled louvres and the divertor field coils are assumed to be maintained at room temperature i.e. 300 K, while the temperature of the vacuum vessel is assumed to be 473 K. The main assumptions on which the present study has been based mainly consist of the axisymmetry in the toroidal direction, the equilibrium of gas mixture (i.e. D and D_2) before entering the sub-divertor area (i.e. assumption of gas at rest with zero incoming velocity), the absence of the volumetric/surface recombination and dissociation processes and finally the constant capture coefficient of the cryopump. Regarding the first assumption, although the authors are aware of the geometrical non-uniformity in the toroidal direction (i.e. no symmetric gas puffing, existence of support structures and diagnostics), it was intentionally decided to take as first step an approach, which requires only modest computational effort (i.e. 2D representation), but already includes some of the complex geometrical characteristics of such a flow domain. A complete 3D modelling, which additionally incorporates the study of the flow between the divertor cassettes, is foreseen as a future action once the feasibility of the present approach is demonstrated. Regarding the latter assumption of the pump modelling, it is noted that in all DIVGAS calculations the boundary conditions, which are assumed on the pumping surface are represented by a given capture coefficient ξ [17], which implies the probability of a particle to be absorbed on this surface. Consequently, ξ varies in the range $0 \leq \xi \leq 1$. It is noted that ξ represents the imposed condition of fixed pumped particle flux and is related with the effective pumping speed S_{eff} of the pumping surface via the following equation

$$S_{eff} = \frac{1}{4} A v_T \xi \quad (1)$$

where v_T is the thermal velocity and A the area of this surface. Based on the fact that the total circumference length of the JET cryopump is 20 m and the height of the pumping surface is 0.3 m [18], the total pumping area is A=6 m^2. Moreover, taking into account that the measured pumping speed of the cryopump is 200 m^3/s for deuterium gas [18] and the surface of the chevron (i.e pumping surface) is at temperature 80 K, then from Eq. (1), it is deduced that the capture coefficient of the pumping surface should be ξ=0.205. In the present study, two values of the capture coefficient were assumed, namely the above estimated value of ξ=0.205 and the ideal case of ξ=1, in which the pump never saturates at maximum possible pumping speed.

3. Experimental setup

All the measurements which are presented in this work correspond to low confinement mode (L-mode) plasma cases with a JET ITER-like wall configuration [16]. The JET ITER-like wall (JET-ILW) consists of Be-coated inconel tiles [19], including bulk Be in high heat flux areas, such as limiters, and Be-coated carbon-fiber composite (CFC) surfaces in the other, recessed areas. The divertor plasma facing components (PFC) are made of bulk W for the horizontally inclined tiles at the low-field side (LFS) and W-coated CFC surfaces in all the other divertor areas, including the vertically inclined targets at both the high-field side (HFS) and LFS. More details about the experimental procedure and main machine parameters can be found in [16]. Furthermore, during the entire pulse series (i.e. JPN 81472-91), as the upstream separatrix density in the LFS mid-plane $n_{e,sep,LFS-mp}$ increases, the response of the neutral gas pressure in the divertor is measured using a pressure gauge. It is noted that in order to reduce the influence of the stray magnetic field on the gauge, the pressure gauge system is located far downwards from the sub-divertor structure (almost 2.5 m away, see Fig. 2a). Both locations communicate through a series of pipes and bellows. The pressure system consists of two capacitance diaphragm gauges. The first device is a MKS 627D Baratron with maximum pressure limit of 1.33 mbar and accuracy in reading of 0.12%, while the second gauge is a Pfeiffer CMR 365 with 0.1 mbar maximum pressure limit and accuracy in reading of 0.5% [20]. It is noted that the latter device due to the low temporal resolution is only used as a cross reference for the former

gauge. As a result, all the used pressure values presented here reflect only MKS 627D Baratron measured data.

4. Numerical modelling of the JET sub-divertor

4.1. The Direct Simulation Monte Carlo algorithm

The DSMC method, on which DIVGAS code is based, consists of a reliable and powerful numerical tool for modelling rarefied gas flows [21-23]. According to this method, a gas flow domain is divided into a network of cells. Initial positions and velocities of a large number of model particles are adopted. Each model particle in the simulation represents a large number of real molecules in the physical system. The motion of particles and their collisions are uncoupled by the repetition of the following steps:

- Free motion of particles is modelled, i.e. their new coordinates $\mathbf{r}_{\mathrm{new}}$ are estimated via the old ones $\mathbf{r}_{\mathrm{old}}$ as
  $$\mathbf{r}_{\mathrm{new}} = \mathbf{r}_{\mathrm{old}} + \mathbf{v}\Delta\mathrm{t}, \quad (2)$$
  where $\mathbf{v}$ is the vector of the molecular velocity. If a particle during the motion crosses a solid surface, then the purely diffuse gas–surface interaction is applied and the particle continues its motion with a new velocity during the rest of time interval $\Delta\mathrm{t}$.
- Intermolecular collisions are simulated following the Non-Time Counter method [10], i.e. the number of pairs to be tested in each cell is calculated as
  $$\mathrm{N}_{\mathrm{coll}} = \frac{1}{2}\mathrm{N}_{\mathrm{p}}\overline{\mathrm{N}}_{\mathrm{p}}\mathrm{F}_{\mathrm{N}}(\sigma_{\mathrm{T}}\mathrm{v}_{\mathrm{r}})_{max}\frac{\Delta\mathrm{t}}{\mathrm{V}_{\mathrm{C}}}, \quad (3)$$
  where N_{p} is the number of particles in a cell at that moment, $\overline{\mathrm{N}}_{\mathrm{p}}$ is the average number of particles in the same cell during all previous steps, F_{N} is the number of real particles represented by one model particle, σ_{T} is the total cross-section of the particle, $\mathrm{v}_{\mathrm{r,max}}$ is the maximum particle relative velocity, and V_{C} is the cell volume. Two particles from the same cell are randomly chosen and they are accepted for collision under the condition $\frac{\mathrm{v}_{\mathrm{r}}}{\mathrm{v}_{\mathrm{r,max}}} > \mathrm{R}_{\mathrm{f}}$, where v_{r} is the relative velocity of this pair and R_{f} is a random number uniformly distributed over the interval [0,1]. If the pair is accepted, their velocities are replaced by new values according to the variable hard sphere (VHS) interaction law [10]. As in the hard sphere model the collision cross section is given by the expression $\sigma_{\mathrm{T}} = \pi d^2$, but now the molecular diameter d is a function of relative speed v_{r}, defined as
  $$d = d_{ref}\left[\left\{\frac{2kT_{ref}}{m_r \mathrm{v}_r^2}\right\}^{\omega-\frac{1}{2}}\Big/\,\Gamma\left(\frac{5}{2}-\omega\right)\right]^{1/2}, \quad (4)$$
  where d_{ref} is the average molecular diameter in a gas at the reference temperature T_{ref}, m_r is the reduced mass of the gas, which is defined as
  $$m_r = m_1 m_2/(m_1 + m_2), \quad (5)$$
  Γ is the Gamma function and the parameter ω is the viscosity index, which characterizes a given gas. In the present work since molecular and atomic deuterium gases were considered, the viscosity index is chosen as $\omega = 0.73$ [24] and $\omega = 0.68$ [24] respectively.
- Sampling of the macroscopic properties is conducted, i.e. the macroscopic quantities are calculated. The number density n, the bulk velocity vector $\mathbf{u}$ and the temperature T in a computational cell are estimated by the following expressions
  $$\mathrm{n} = \frac{\mathrm{N}_{\mathrm{p}}}{\mathrm{V}_{\mathrm{C}}}\mathrm{F}_{\mathrm{N}}, \mathbf{u} = \frac{1}{\mathrm{N}_{\mathrm{p}}}\sum_{\mathrm{i}=1}^{\mathrm{N}_{\mathrm{p}}}\mathbf{v}, \mathrm{T} = \frac{\mathrm{m}}{3\mathrm{kN}_{\mathrm{p}}}\sum_{\mathrm{i}=1}^{\mathrm{N}_{\mathrm{p}}}(\mathbf{v}-\mathbf{u})^2, \quad (6)$$
  respectively. The final values of these quantities are given by the average amount during all time intervals $\Delta\mathrm{t}$.

In the above framework, an unstructured computational grid, which consists of $5\mathrm{x}10^4$ triangular cells, was applied in the computational field (Fig. 2b). In all the present simulations an optimum value

of $\Delta t = 0.1$ μs has been used, which takes into account the fundamental criterion of DSMC that Δt should be a fraction of the mean collision time. On the other hand, the average number of particles in each cell of the flow field was ranging around 50 particles per cell. This number assures that the statistical scattering of macroscopic quantities along the computation domain is sufficiently low. All the above parameters were chosen to maintain the accuracy of the calculated results within two significant digits. In addition, the Larsen–Borgnakke model [25], which describes the energy exchange between translational and internal degrees of freedom during binary collisions of diatomic molecular deuterium among the gas mixture, is considered. Furthermore, the particle-wall interactions are assumed to be purely diffuse, namely the reemitted particles forget their previous information and are reflected back to the flow domain with a Maxwellian distribution function based on the wall temperature. It is noted that, in the present algorithm the recombination and dissociation processes are not taken into account and therefore, when a D_2 molecule or a D atom hits a wall surface, it remains as a molecule or as an atom respectively. The DIVGAS code used in the present work has been implemented in OpenFOAM [26], an open-source C++ toolbox for computational fluid dynamics. This solver, which is called dsmcFoam, has been rigorously validated for a variety of benchmark cases [27] and it has been modified accordingly for the purpose of the present work. The present DIVGAS code is fully parallelized and for all the presented calculations a high-performance computer named "bwUniCluster" was used, by utilizing up to 128 cores for each case.

4.2. EDGE2D-EIRENE simulations

The scrape-off layer in attached, partially detached and fully detached divertor plasmas obtained at the low field side (LFS) divertor target were previously simulated using the edge fluid code EDGE2D-EIRENE [5,6] as described in Ref. [16]. The experimental data and EDGE2D-EIRENE predictions shown throughout this publication are entirely based on the work presented in [16]. The magnetic configuration corresponds to a low upper-triangularly ($\delta \sim 0.2$) with the high field side (HFS) strike point on the vertical target and the LFS strike point on the horizontal target. In the simulations the electron density at the upstream separatrix was varied by deuterium gas fuelling from the top and the divertor (private flux) regions. Consequently, low-density ($1x10^{19}$ m^{-3}), high-temperature (40 eV) divertor plasmas at the LFS divertor target were obtained at low upstream electron density ($8x10^{18}$ m^{-3}), and high-density ($3x10^{20}$ m^{-3}) and low-temperature (3 eV) at intermediate densities ($1.5x10^{19}$ m^{-3}) at the onset of detachment (figure 11 of Ref. [16]). The EDGE2D-EIRENE predicted ion and power fluxes to, and the electron temperatures at the LFS target are consistent within a factor of 2 of the measured parameters for these upstream electron densities. Reduced electron densities (< 1.0 $x10^{19}$ m^{-3}) and sub-eV electron temperatures were predicted for the highest upstream electron densities (> 2.0 $x10^{19}$ m^{-3}). The predicted low temperature conditions at the LFS divertor plate are consistent with line ratio analyses of line-integrated, high-n deuterium Balmer emission [28]. However, measurements of the total radiated power (Fig. 11b and d of Ref. 15) and the line-integrated deuterium emission of low-n Balmer lines [29] showed a radiation shortfall, which could potentially be due to significant differences in the actual and predicted neutral distribution in the divertor. In addition, significantly higher electron densities are inferred from Stark broadening analyses of line-integrated high-n deuterium Balmer lines across the divertor plasma compared to low electron densities at the LFS divertor plate. In contrast, EDGE2D-EIRENE presently predicts the electron densities to peak at the plate. Addressing the latter two issues is beyond the scope of this publication. Here, the existing EDGE2D-EIRENE predictions as given in Ref. [16] are taken as they stand, and the DIVGAS analyses presented here will be re-evaluated when these issues are resolved.

The Monte-Carlo neutrals code EIRENE [6] is used as inputs to predict the atomic and molecular deuterium fluxes to the divertor wall surfaces, including the neutral fluxes representing the pumping plena on the HFS and LFS divertor corners (Fig. 2b). In these EDGE2D-EIRENE simulations, the sub-divertor structure is not included, and the neutral fluxes into the sub-divertor are determined by the albedos of the assumed pumping plena. Here, the divertor corners are assumed pumping at 6% of the

incoming atomic and molecular fluxes. In addition, EIRENE provides the neutral fluxes to by-pass leaks between toroidal gaps along the vertical targets (Fig. 2a) assuming zero pumping across these gaps [14].

5. Results and discussion

In this section, the results obtained from the DIVGAS calculations and their comparison with corresponding experimental results from the pressure gauge are presented for different plasma collisionality cases. An investigation of neutral gas dynamics, which consist of a parametric analysis of the flow field based on macroscopic parameters of practical interest, is conducted.

5.1. Neutral gas dynamics in the JET sub-divertor

In Fig. 3a, the comparison between the calculated DIVGAS and measured pressure at the gauge location, as a function of the upstream electron density at the LFS mid-plane $n_{e,sep,LFS-mp}$ is presented. As described in [16], by increasing $n_{e,sep,LFS-mp}$, the pressure at the gauge location increases exponentially over two decades. A similar behaviour is reproduced by the DIVGAS results for the case of ξ=0.205 and 1. For the former capture coefficient a factor of five difference between numerical and experimental results is obtained, while for the latter ideal case a no more than a factor of two difference is observed.

In Fig. 3b, the experimental maximum electron density in the LFS divertor target and the sub-divertor pressure (i.e pressure measured by the pressure gauge) versus the separatrix upstream plasma density is presented. When the plasma is fully detached, the outer divertor target density drops at the highest upstream density and so does the sub-divertor pressure. The pressure in the divertor region (and in the sub-divertor) decreases, as a result of an expansion of the neutral region in the divertor leg. As the ionisation front moves off the divertor plate, the region in which the neutrals exist expands significantly across the divertor leg and towards the installed cryopump. The scaling of the sub-divertor pressure with the upstream plasma density includes all the plasma physics from the outer midplane to the divertor, which is still a complex issue to address.

For a better understanding of the neutral gas dynamics in the area of the sub-divertor, a calculation of macroscopic quantities of practical interest in various locations (probes) along the flow domain has been performed. In Fig. 2b, the five representative locations, which cover a wide area of the sub-divertor, are depicted. For each of these points, the local neutral pressure and temperature of gas mixture and the corresponding local Kn number have been estimated. The local Kn number is defined as the ratio of the local mean free path, over a characteristic length of the flow, which is in this case the average of the two cell lengths. The mean free path λ_{VHS} is obtained by the following expression,

$$\lambda_{VHS} = \left\{\sqrt{2}\pi d_{ref}^2 n\left(T_{ref}/T\right)^{\omega-1/2}\right\}^{-1}, \quad (7)$$

where *n* and *T* is the local number density and temperature respectively.

In Fig. 4a, the gas mixture temperature in the above-defined locations is presented predicting that the temperature in the sub-divertor area is almost independent of the plasma conditions and strongly depends on the defined temperature of the stationary walls. Moreover, the flow field is shown to be non-isothermal with the temperature to range from 300 to 450 K. In Fig.4b, the estimated Kn number in the five different locations in terms of the upstream density is presented. It indicates that for the case of low $n_{e,sep,LFS-mp}$, the Kn number is high and varies between 10^2 to 10^3, which indicates that the flow is highly rarefied and is in the collisionless regime. On the other hand, as $n_{e,sep,LFS-mp}$ increases, the Kn number decreases almost two orders of magnitude until the transition regime (Kn$\sim$1) is established. In this regime, the presence of the intermolecular interactions becomes an important factor for the prediction of the macroscopic quantities. In addition, it is noted that the Kn number especially in the location #2 for the low and medium density cases is always decreased due to the high incoming particle flux injected from the Lower-LFS gap. On the other hand in locations #3, #4 and #5 the Kn number is predicted to have almost the same magnitude. The same observation can be visualized in Fig.5a, where the pressure of the gas mixture (i.e D and D_2) is presented. Since

pressure is inverse proportional to the Kn number, it is deduced that the pressure variation along the flow field follows qualitatively this trend.

Another significant observation in such a complex geometry is the difference between the measured pressure in the pressure gauge location and the calculated one in the sub-divertor area (location #3), shown in relative terms versus the upstream density in Fig. 5b. Based on this plot, it is predicted that as the divertor upstream density increases, the relative difference between the pressure gauge and #3 location decreases and lies between 20 to 35% for the case of the considered flow, i.e the pressure in location #3 is always higher than in the gauge location, for each gas species. Since the vertical downpipe is closed with a gate valve, no mass flow rate is expected along it, in steady-state conditions. The conductance of the pipe is almost zero and the pressure difference occurs mainly due to temperature difference and only at low collisionality flow cases. By calculating the local Mach number in the whole flow domain, indeed the Mach number in that region is of the order of 0.01, which implies a gas at rest. This strong effect is for the first time quantified and it is suggested to be used in the evaluation of future pressure measurements, or in the re-evaluation of previous experimental data.

In Fig. 6, the molar concentration of molecular deuterium in the whole flow domain, which is defined as

$$C_{D_2} = \frac{n_{D_2}}{n_D + n_{D_2}}, \quad (8)$$

with n_{D_2} and n_D the local number densities of molecular and atomic deuterium respectively, is presented. In the absence of atomic recombination on the walls of the sub-divertor, it is seen that for the lowest upstream plasma density and either for ξ=0.205 or 1, the concentration of molecular deuterium in the whole flow domain is of the order of 60% (Fig. 6a), while for higher plasma density cases this percentage drops to 30% (Fig. 6b). In real operational conditions, most of the atomic deuterium will be recombined to molecular deuterium on the wall surfaces and finally only molecualr deuterium will be observed, particularly in the lower part of the sub-divertor. The influence of atomic physics on the whole flow field is part of an on going activity, which includes further developement of the DIVGAS code.

5.2. Neutral recirculation in the JET sub-divertor

An important qualitative observation regarding the behaviour of the flow field depending on the operational upstream conditions is the recirculation of neutrals, which takes place through the inlet boundaries for all the upstream plasma densities examined in this work. In Fig. 7a, the gas mixture streamlines for the case of low-density case is presented and it is observed that only in the Lower-HFS gap gas mixture is going towards the plasma chamber (see the direction of streamlines). The particle flux, which flows towards the plasma region, is equal to 1.7×10^{18} ($s^{-1}m^{-1}$). In the case of medium density case, recirculation of neutral gas mixture takes place in the Lower-HFS and in the Upper-LFS gap as shown in Fig. 7b, with the particle flux to be equal to 8.4×10^{18} ($s^{-1}m^{-1}$) and 1.3×10^{19} ($s^{-1}m^{-1}$) respectively. On the other hand, for the high-density case (Fig. 7c) recirculation of gas mixture takes place only in the Upper-LFS gap behind the divertor vertical targets. The calculated particle flux for that case is equal to 4×10^{19} ($s^{-1}m^{-1}$). It is noted that for all the above cases the neutral recirculation behind the divertor tiles is two or even three orders of magnitude lower than the ion recycling flux to the walls and therefore the influence of neutral particles on the overall divertor particle balance is assumed to be negligible. On the other hand, it is necessary to be considered that for the case of even higher divertor densities, the recirculation neutral particle fluxes might not be as low as the ones currently presented and therefore special attention should be given in taking into account such contribution on the divertor plasma edge modelling.

6. Summary

The present work includes a numerical study of the neutral gas dynamics in the JET sub-divertor. A realistic 2D (poloidal) model of the sub-divertor geometry is applied. The experimental data represent the neutral gas pressure obtained by the pressure gauge (which is located ~2.5 m below the cryopump) for an L-mode plasma case. The DIVGAS code is able to quantitatively predict the behaviour of the flow domain including macroscopic quantities of practical interest as the pressure and temperature und bulk velocity. The numerical pressures in the sub-divertor area differ by a factor of two as long as an ideal pump is assumed, while the difference increases to a factor of five whenever a more realistic pump is considered. For all the presented plasma cases, the flow pattern is non-isothermal and a factor of two relative difference of temperature distribution for different plasma conditions is obtained. The relative difference between the measured neutral pressure at the pressure gauge location and the pressure in the centre of sub-divertor structure varies between 20-35 % depending on the upstream plasma conditions. Furthermore, for low, medium and high upstream density simulations, recirculation of neutrals occurs through the gaps between the target tiles. The recirculation particle flux for these cases is assumed to be negligible compared with the recycling ion flux on the walls. However, the influence of neutral recirculation on divertor plasma conditions is expected to be more significant for higher collisionality divertor conditions.

The value of the presented workflow of modelling the JET sub-divertor is based mainly on the fact that the DIVGAS code is benchmarked under a known geometrical structure and it can be further exploited in the design and optimisation of the DEMO and JT-60SA divertors, in which it is expected that higher densities (i.e lower Knudsen numbers) will be present. Therefore, a more appropriate description of the neutral intermolecular interactions should be greatly considered. Additionally, the DIVGAS code is proven to be a suitable tool for the understanding of the particle exhaust system and the role of pumping as plasma actuator in a tokamak. Finally, the DIVGAS code can be further applied as benchmark tool for any new proposed algorithm, which includes neutral particle interactions.

Acknowledgements

This work has been carried out within the framework of the EUROfusion Consortium and has received funding from the EURATOM research and training programme 2014-2018 under grant agreement No 633053. The views and opinions expressed herein do not necessarily reflect those of the European Commission. Moreover, this work was performed on the computational resource bwUniCluster funded by the Ministry of Science, Research and Arts and the Universities of the State of Baden-Württemberg, Germany, within the framework program bwHPC.

References

[1] COLCHIN, R., et al., “Effects of particle exhaust on neutral compression ratios in DIII-D”, J. Nucl. Mater., **266-269**, (1999) 472-477.

[2] NIEMCZEWSKI, A., et al., “Neutral particle dynamcis in the Alcator C-MOD tokamak”, Nucl. Fusion, **37** (2), (1997), 151-163.

[3] KUKUSHKIN, A., et al., “Analysis of performance of the optimized divertor in ITER”, Nucl. Fusion, **49**, (2009) 075008.

[4] SCARABOSIO, A., et al., “Measurements of neutral gas fluxes under different plasma and divertor regimes in ASDEX Upgrade”, J. Nucl. Mater., **390-391**, (2009) 494-497.

[5] WIESEN, S., ITC-Report, http://www.eirene.de/e2deir_report_30jun06.pdf, (2006).

[6] REITER, D., et al., “The EIRENE manual", http://www.eirene.de.

[7] KOTOV, V., et al, “Numerical study of the ITER divertor plasma with the B2-EIRENE code package", Jülich-Report 4257, (2007).

[8] BHATNAGAR, P. L., GROSS, E. P., and KROOK, M., “A model for collision processes in gases. I. Small amplitude processes in charged and neutral one-component systems”, Phys. Rev., **94**, (1954) 511.

[9] SHARIPOV, F., SELEZNEV, V., “Data on Internal Rarefied Gas Flows”, J. Phys. Chem. Ref.

Data, 27 (3), (1998).
[10] BIRD G. A., *Molecular Gas Dynamics and the Direct Simulation of Gas Flows*, Oxford University Press, (1994).
[11] LOARTE, A., "Effects of divertor geometry on tokamak plasmas", Plasma Phys. Control. Fusion, **43**, (2001) 183-224.
[12] STOTLER, D. P., LABOMBARD, B., "Three-dimensional simulation of gas conductance measurement experiments on Alcator C-Mod", J. Nucl. Mater., 337-339 (2005) 510-514.
[13] LISGO, S., et al., "OSM-EIRENE modeling of neutral pressures in the Alcator C-Mod divertor", J. Nucl. Mater., **337-339**, (2005), 139-145.
[14] MOULTON, D., et al., "Pumping in vertical and horizontal target configurations on JET in L-mode; An interpretive study using EDGE2D-EIRENE", Proceedings of the 42nd European Physical Society Conference on Plasma Physics, EPS 2015, Lisbon, Portugal (2015).
[15] GLEASON-GONZALEZ, C., et al., "Simulation of neutral gas flow in a tokamak divertor using the Direct Simulation Monte Carlo method", Fus. Eng. Des., **89**, (2014) 1042-1047.
[16] GROTH, M., et al., "Impact of carbon and tungsten as divertor materials on the scrape-off layer conditions in JET", Nucl. Fusion, **53**, (2013) 093016.
[17] HAEFER, R.A., "Cryopumping", Clarendon Press, Oxford (1989).
[18] OBERT, W., et al., "Performance of the JET pumped divertor cryopumpsystem", 16th IEEE/NPSS Symposium, doi: 10.1109/FUSION.1995.534329, (1995) 742-745.
[19] BREZINSEK, S., "Plasma-surface interaction in the Be/W environment: Conclusions drawn from the JET-ILW for ITER", J. Nucl. Mater., (accepted).
[20] KRUEZI, U., et al., "JET divertor diagnostics upgrade for neutral gas analysis", Rev. Sci. Instrum., **83**, (2012), doi: 10.1063/1.4732175.
[21] VAROUTIS, S., et al., "Rarefied gas flow through channels of finite length at various pressure ratios", Vacuum, **86**, (2012) 1952-1959.
[22] VAROUTIS, S., DAY, CHR., "Numerical modelling of an ITER type cryopump", Fus. Eng. Des., **87**, (2012) 1395-1398.
[23] VAROUTIS, S., et al., "Rarefied gas flow through short tubes into vacuum", J. Vac. Sci. Technol. A, **26**(2), (2008) 228-238.
[24] ASSAEL, M. J., MIXAFENDI, S., WAKEHAM, W. A., "The Viscosity and Thermal Conductivity of Normal Hydrogen in the Limit of Zero Density", J. Phys. Chem. Ref. Data, 15(4), (1986) 1315-1322.
[25] BORGNAKKE, C., LARSEN, P. S., "Statistical Collision Model for Monte Carlo Simulation of Polyatomic Gas Mixtures", J. Comp. Phys., **18**, (1975) 405–420.
[26] OPENFOAM®, http://www.openfoam.com/ .
[27] SCANLON, T. J. et al., "An open source, parallel DSMC code for rarefied gas flows in arbitrary geometries", Computers and Fluids, **39** (10), (2010) 2078-2089.
[28] LOMANOWSKI, B. A. et al., "Inferring divertor plasma properties from hydrogen Balmer and Paschen series spectroscopy in JET-ILW", Nucl. Fusion, **55**, (2015) 123028.
[29] LAWSON, K. D. et al., "Improved EDGE2D-EIRENE simulations of JET ITER-like wall L-mode discharges utilising poloidal VUV/visible spectral emission profiles", J. Nucl. Mater., 463 (2015) 582.

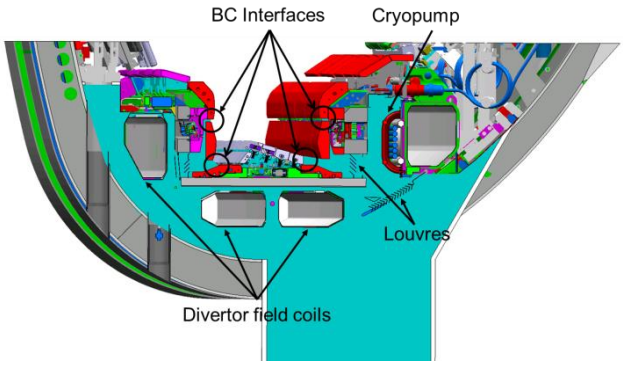

Figure 1: Geometrical representation of JET sub-divertor structure.

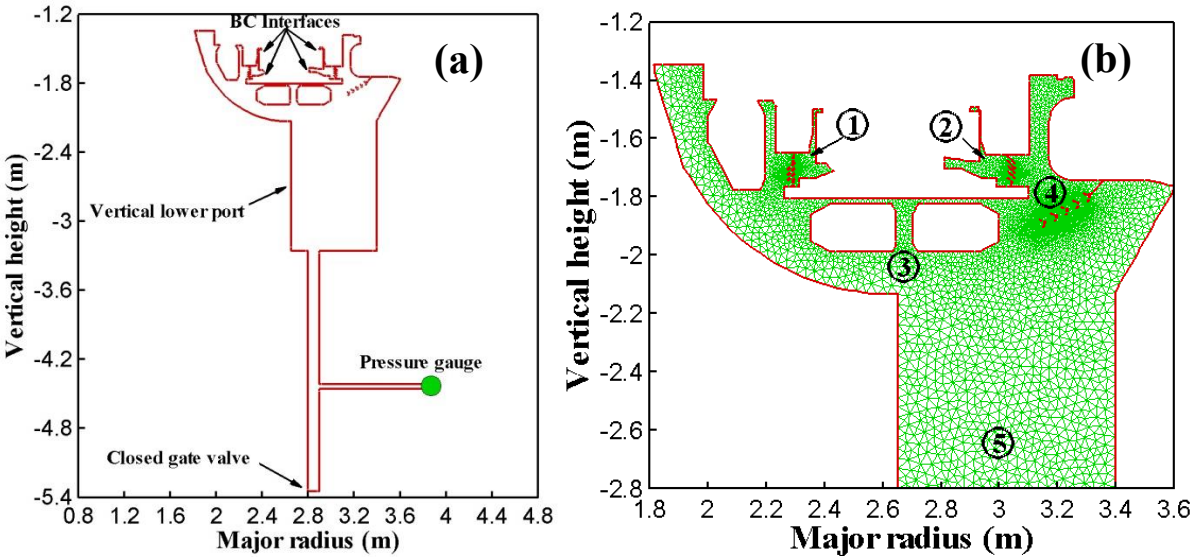

Figure 2: (a) 2D model of the JET sub-divertor. (b) Various locations (probes) in the sub-divertor area.

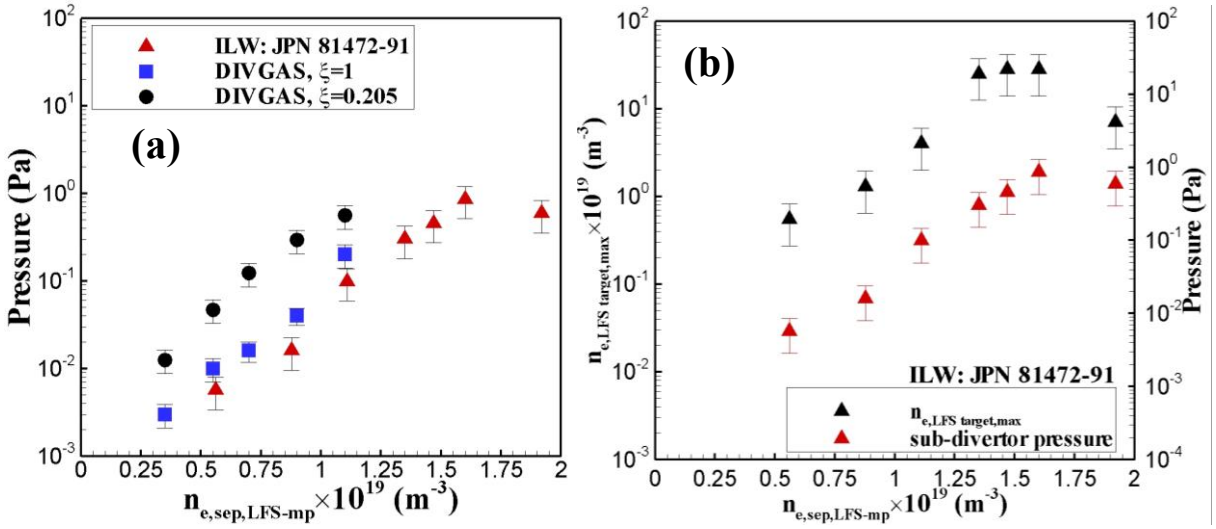

Figure 3: (a) Comparison between the DIVGAS and experimental molecular deuterium pressure in the location of the pressure gauge. (b) The experimental maximum electron density in the LFS divertor target and the sub-divertor pressure versus the separatrix upstream plasma density.

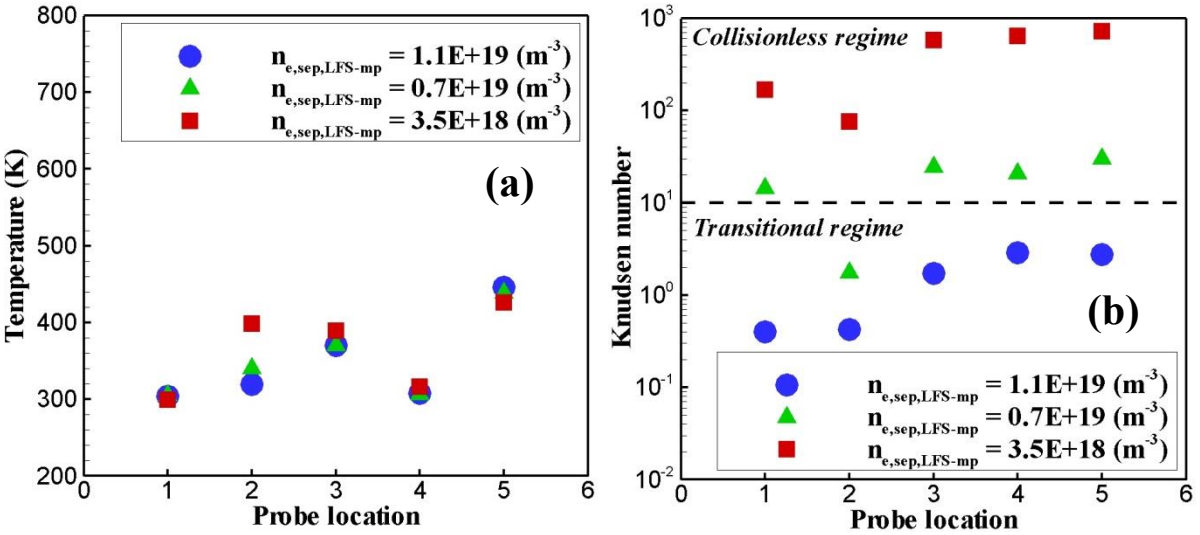

Figure 4: (a) Overall temperature and (b) the local Kn number for the gas mixture in various locations of the sub-divertor for ξ=1.

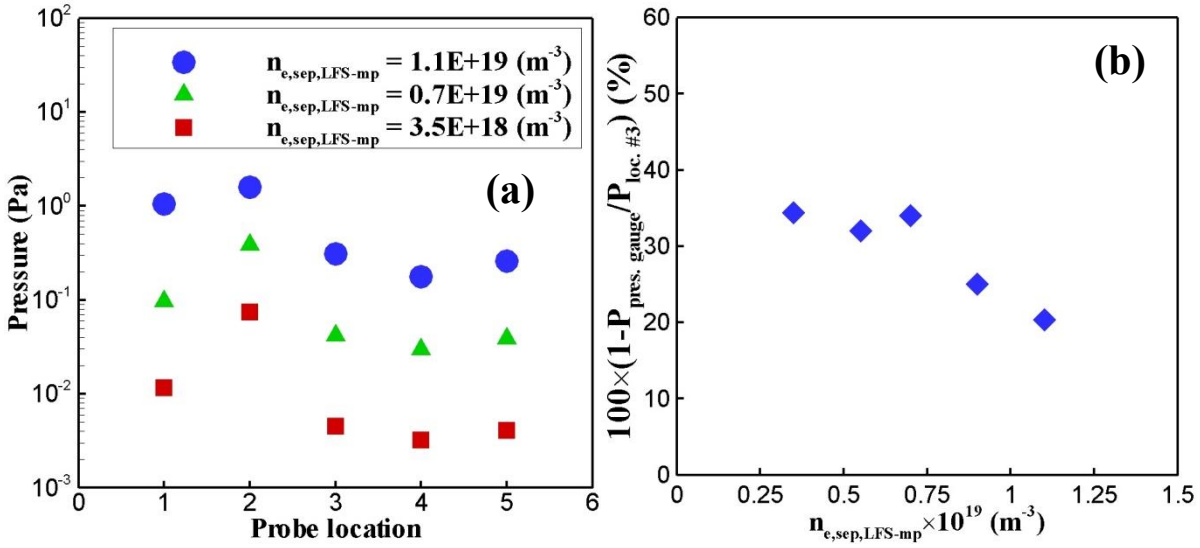

Figure 5: (a) Pressure for gas mixture in various locations of the sub-divertor for ξ=1. (b) Relative difference between the pressure at the gauge and the pressure at location #3 in the lower middle part of sub-divertor for ξ=1.

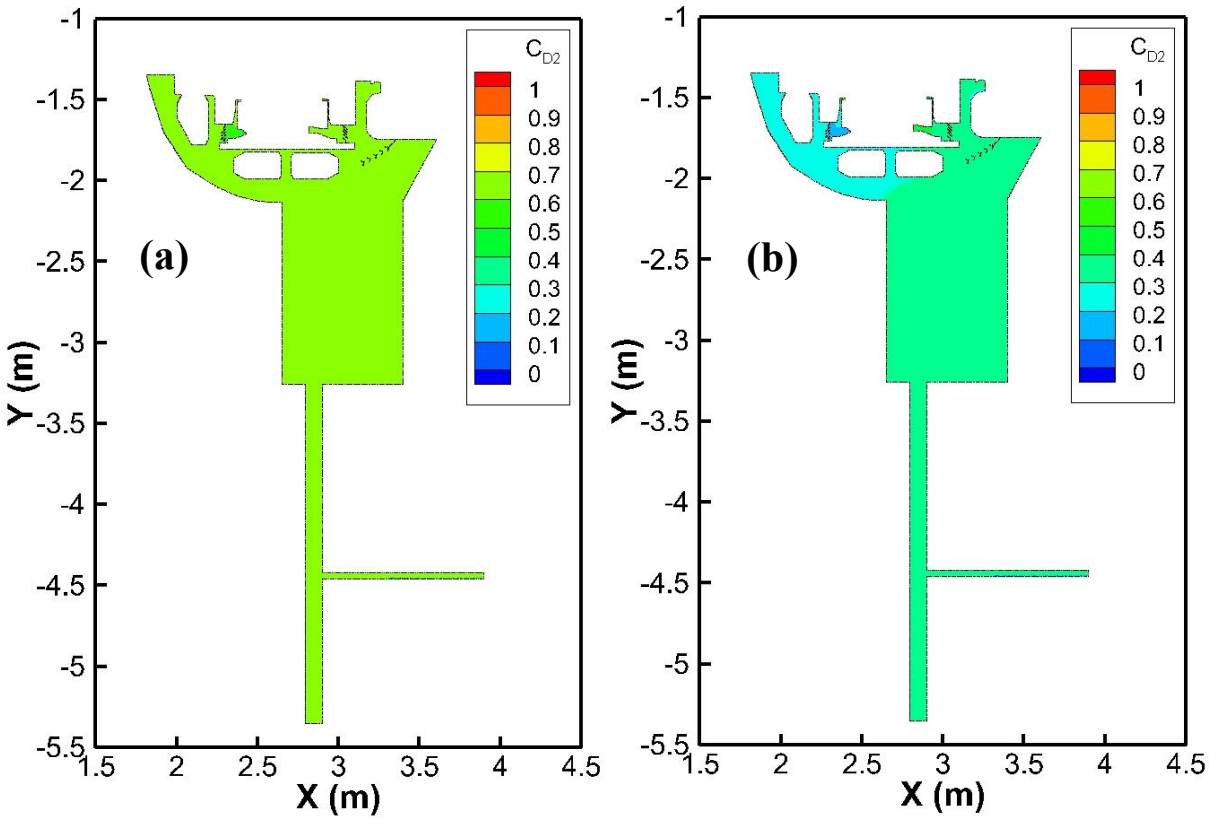

Figure 6: (a) Molar concentration of molecular deuterium for $n_{e,sep,LFS\text{-}mp}$= 3.5x10^{18} m^{-3} and ξ=0.205. (b) Molar concentration of molecular deuterium for $n_{e,sep,LFS\text{-}mp}$= 1.1x10^{19} m^{-3} and ξ=0.205.

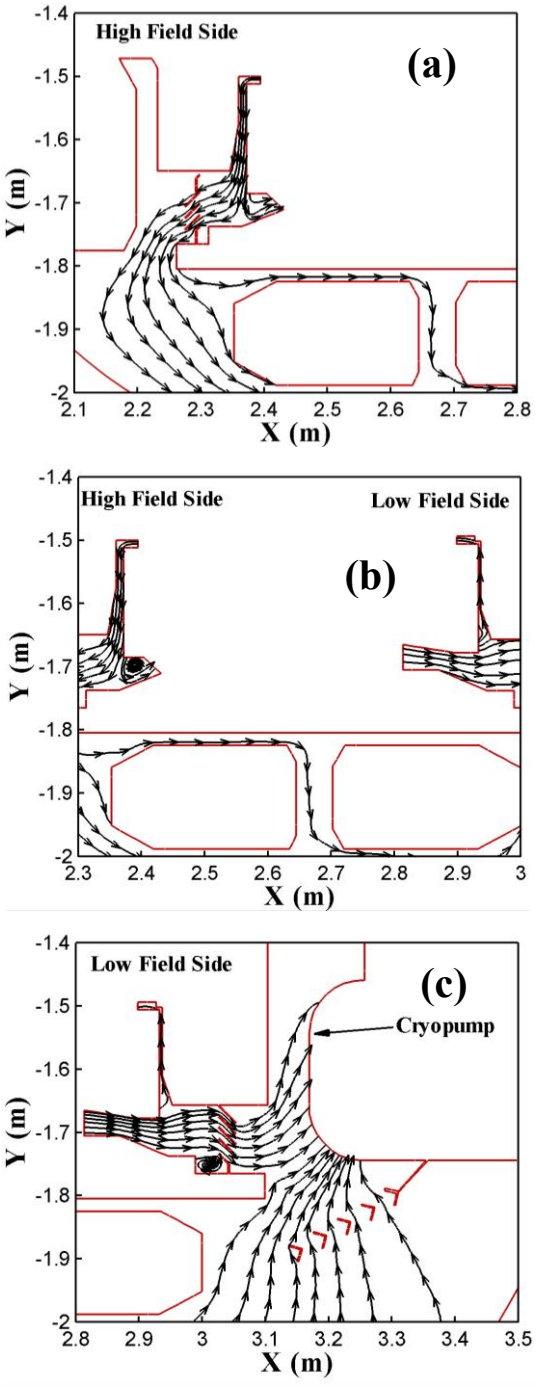

Figure 7: Streamlines of mixture (D and D_2), for the following separatrix upstream plasma density cases: (a) $n_{e,sep,LFS\text{-}mp}$= 3.5x10^{18} m^{-3}, (b) $n_{e,sep,LFS\text{-}mp}$=0.7x10^{19} m^{-3} and (c) $n_{e,sep,LFS\text{-}mp}$=1.1x10^{19} m^{-3}. For all cases the capture coefficient is equal to ξ=1.